Perturbative Effects of Extra-Solar Matter on Oort Cloud Orbits

Evan Dowling Mentor: Prof. Asantha Cooray

Abstract:

The Oort Cloud, a set of comets orbiting the sun at very long distances, forms an interesting testing ground for various theoretical models of the galaxy and the Solar system. Oort Cloud objects, because they are so distant from the sun, are extremely sensitive to the solar system's interaction with external galactic matter. The system is analytically complicated, but can be analyzed in a detailed way by utilization of a numerical simulation. We examine the perturbative effects of extra-solar matter on orbits with stable non-perturbed initial conditions. The most well-known external actor on the solar system is the remainder of the galaxy. Aside from nearby passing stars, a very rare occurrence, the solar system is perturbed by two basic galactic forces, that exerted by the bulge at the center of our galaxy, and that exerted by the Galactic disk, a two dimensional distribution of matter along the galactic plane. Additionally, we explore the effects of dark matter sub-haloes of various masses on both the unperturbed and the perturbed orbits. By subjecting initially stable orbits in the un-perturbed case, we establish a baseline for the relative effectiveness of each interaction type, and examine the resultant changes in both comet cloud demographics as well as observable comet flux. The effects of extra-solar matter on the Oort comet Cloud can, in the right combination of both initial conditions and galactic density functions, exhibit behavior similar in magnitude to that provided by observation.

Introduction:

The Oort Cloud

The Oort Cloud is an immense spherical cloud of comets orbiting the sun with semi-major axes between 20,000 and 100,000 AU. The Oort Cloud was first inferred by the Dutch Astronomer Jan Oort in 1950.[[1]] Although not directly observable by telescope, astronomers are fairly confident of its existence through the measurement of long-period comets and their points of origin. The cloud itself is thought to contain many objects with a total mass near 40 times that of the Earth.[[11]] Recently, the Oort Cloud has gotten more attention from cosmologists who seek to use the Oort Cloud as a testing ground for various models of the galaxy. It is useful for this sort of investigation because the solar gravitational forces are very weak, thereby increasing the relative magnitude of extra-solar perturbations.

The Galactic Model

In examining these perturbative effects, it is necessary to formulate an exact model of the Galaxy. In essence, the current model analyzes the visible component pof the galaxy as a superposition of two essential effects: gravity exerted by a bulge in the center of the galaxy, and gravity caused by the accreted disc lying along the galactic plane. The sun itself orbits the center of the Milky Way on a near circular orbit of radius 8.5 kpc. At this distance the sun encloses 1.4 x 10^{11} solar masses in the galactic bulge.[[2]] This enclosed mass value includes the portion of the dark halo enclosed by the sun, as well as the luminous matter concentrated at the galactic center. Due to the exceptionally high mass of the central bulge, objects within the Oort Cloud are affected nearly as much by external mass as they are by the sun itself. Since the sun lies essentially on the galactic plane, the galactic disc exerts an oscillatory force on the sun causing it to exhibit sinusoidal behavior across the galactic plane. These oscillations can effectively "shake" comets out of orbit.

Dark Matter:

The existence of large quantities of unseen mass in galaxies was first inferred by astronomer Fritz Zwicky, who noticed that galaxies orbit each other at velocities corresponding to masses 400 times their estimate based on luminosity profiles. However, this theory was widely rejected by the scientific community until in the 1960's Vera Rubin began investigating the rotation curves of the Andromeda Galaxy. In her analysis, she found that in order for the arms of the spirals to maintain their shape the angular speed of particles in those arms suggested a distribution of mass in the galaxy vastly different from that shown by luminosity profiles.[[7]] These results not only suggest the existence of Dark Matter, but by examining the rotation curve of a galaxy it is additionally possible to determine the distribution of matter in that galaxy. Assuming that visible matter comprises the entirety of the galaxy would suggest, by Newton's laws, that the predicted rotation curve would follow a $V(R) \propto \frac{1}{\sqrt{R}}$ relation.

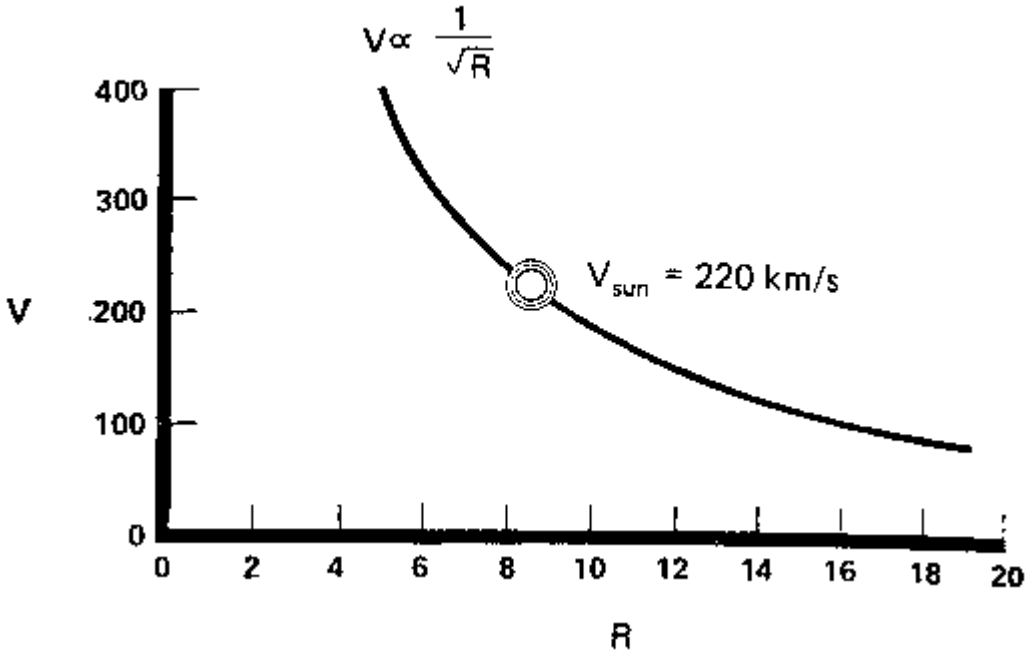

Figure 1: Courtesy of http://ircamera.as.arizona.edu/astr_250/Lectures/Lec_22sml.htm

However, the observed rotation curve of the Milky Way Galaxy is quite different, suggesting that either Newtonian gravitation is inaccurate at large distances, or that the distribution of mass in the galaxy is vastly different from that predicted by luminosity estimates.

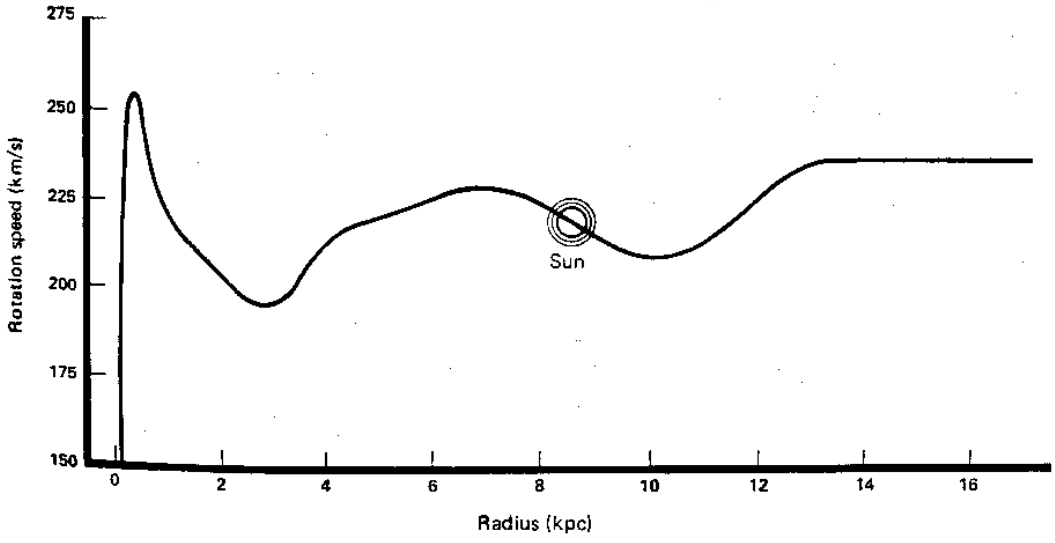

Figure 2: Courtesy of http://ircamera.as.arizona.edu/astr_250/Lectures/Lec_22sml.htm

Using the observational data, it is possible to determine a distribution of "hidden mass" from the deviating rotation curve using the virial theorem, additionally, it is possible to determine from these estimates approximately how much "Dark Matter" is enclosed by the solar orbit. All in all, current estimates cite a net dark halo of mass $M_H \approx 4 \times 10^{11} M_*$.[[8]] Additionally, astronomers predict a non-uniform spherical mass distribution of $\rho_H = \rho_D \frac{1}{1 + {}^{r}/_{r_H}{}^2}$.[[3]] The mass of the entire dark halo is theorized to be comprised of many different possible candidates. A popular current candidate for dark halo mass is that of "baryonic dark matter." Primarily this particular form of Dark Matter takes the form of Massive Compact Halo Objects, or MACHOs. [[9]] The question of course is, if there is MACHO Dark Matter in the Milky Way, then how much is there, and, in what sized quantities does it occur. Gravitational Lensing techniques have recently produced interesting results in the detection of MACHOs. An experiment started in the mid-1990's has yielded detections of several probable MACHOs in the inner galactic region.[[10]] However, the study cannot conclusively determine the existence of sub-halo objects. Many of the potential candidates have been discredited as binary events or other stellar phenomena. However, as time goes on and micro-lensing data becomes more complete, there does appear to exist a degree of evidence that MACHOs exist if perhaps not in the numbers once postulated. Current theory predicts a MACHO fraction of the net halo mass between 10% and 20%. The detected candidates suggest a mass distribution amongst halo objects between .05 and 1 solar mass. By solving the halo density function for the solar position and multiplying it by the MACHO fraction we attain the MACHO mass distribution in the solar vicinity about 0.01 Solar Masses per cubic parsec.[[12]] Dividing this mass density by the mean MACHO mass gives the MACHO number density which can be used in a Monte Carlo type numerical simulation.

The effects of Dark Matter sub-Haloes on both observable flux and cloud population are varied, primarily dependent upon the chosen masses of the haloes and the likelihood of their generation. Current theory suggests a number distribution of sub-haloes with an upper bound at 1 Solar mass and an absolute lower bound at one Earth mass.[[4]] Cosmologists believe that MACHOs below this mass threshold would be evaporated over a galactic time scale. Use of Solar massed haloes in the simulation parameters tends to depopulate the cloud very rapidly, while Earth massed haloes have almost no perceivable effect whatsoever. There are, in essence, two effects at work here. The increased mass of the haloes increases the efficacy by increasing the force magnitude, but also, since massive haloes are less frequent than light haloes, massive halo generation routines create a less symmetric distribution of mass. Essentially, the mass of the halo determines the "lumpiness" of the MACHO field. However, another important factor in the efficacy of the sub-haloes is their velocity relative to the sun. Higher velocities cause haloes to pass through the solar system more quickly, giving them less opportunity to perturb orbits. These velocities are generated using a Maxwellian Distribution with a peak at about 150 km/s along each coordinate axis, giving a net mean magnitude of 240 km/s.[[5]] The third factor affecting the magnitude of halo perturbations is the distribution of impact parameters. In our simulation, we chose to disregard accelerations of the halos, thus, halos follow linear trajectories. So, if haloes are generated by calculating a random angle of incidence less than orthogonal to the initial position vector, the impact parameters will follow a distribution given by:

$$g(y) = \frac{2}{R\pi} \frac{1}{\sqrt{1 - \frac{y^2}{R^2}}}$$

A histogram output from the initial conditions of the generated haloes gives a distribution of:

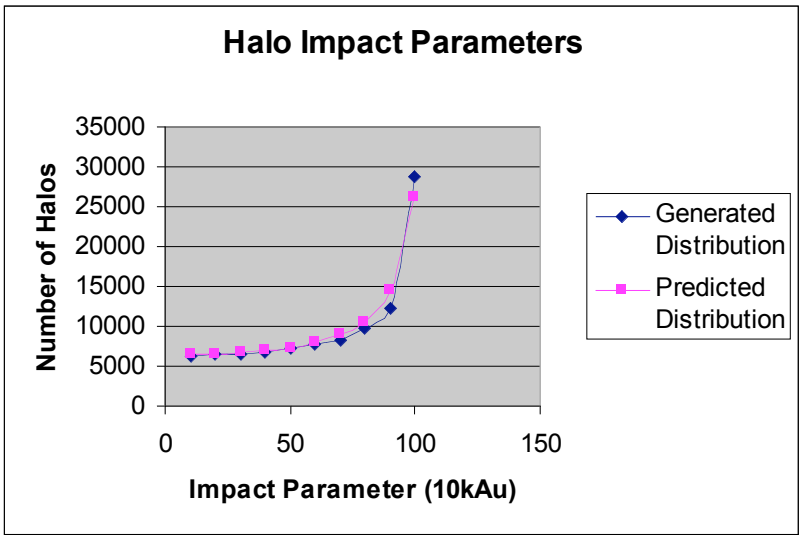

Figure 3: Halo Impact Parameters

Galactic Effects and the Oort Cloud:

Objects with stable orbits in the Oort Cloud are nearly impossible to observe. They are cold and emit no light of their own, furthermore they have no nearby light sources to reflect, in fact, the only Oort Cloud objects ever observed have been observed outside of the Oort Cloud. These observed orbits are theorized to be destabilized orbits that have lost or gained enough energy to enter an observably close trajectory to the sun. Thus, it is interesting to investigate whether or not the current model of galactic structure can account for these observable phenomena.

Since the forces involved can become very complicated, it is unreasonable to expect an exact analytical analysis of the problem. However, using a numerical simulation it is possible to observe the interactions in a meaningful way. The process is to generate acceleration functions, stable initial conditions, and then utilize a fourth order Runge-Kutta numerical solution to plot the perturbed orbits as a function of time. Using these data points it is possible to attain a theoretical value for the flux of comets into the observable range.

The Simulation:

Setting up the simulation requires several additional pieces of knowledge. Foremost, it needed to be variable in terms of which interactions were being considered. This was necessary so that we could analyze the various aspects of the model and their effects in an isolated manner. Comparison of plots for identical initial conditions but varied perturbative forces gives a baseline for an understanding of how the individual aspects of the model physically change the system. Thus, the simulation contains several true false switches which allow all interactions besides those of the sun to be "switched on and off."

Additionally, it is necessary to either provide an initial condition and numerically model the motion of the sun through the galaxy or find an analytical solution to the equations of motion.

However, predefining an analytical path for the sun subjects comets to a degree of propagating numerical error that the sun is not subjected to. Thus, it is more consistent to simply integrate the path of the sun along with the path of the comets. For purposes of optimization, this path can be integrated once at startup and then be saved for further reference.

In the data collection for this simulation we chose to integrate sets of 1000 randomly generated orbits for each possible combination of chosen interactions. This data would then be placed through post processing software which sorts data into bins of distance, and identifies observable orbits. Furthermore, it is useful to compare which initial conditions correspond to bound orbital states.

The Coordinate System:

In this particular analysis we use a coordinate system centered at the galactic center with z = 0 defining the galactic plane, and (x,0,0) indicating the initial position of the sun.

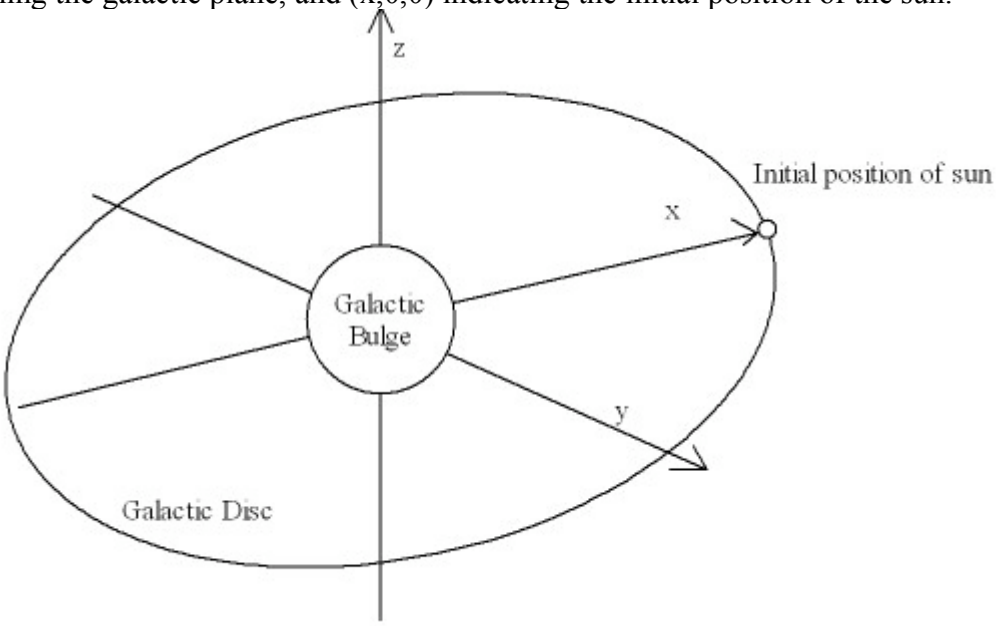

Figure 4:Coordinate System Diagram

Generating Stable Orbits:

Initially, it is useful to develop a set of criteria which determine whether or not an orbit is stable and remains within a radial upper and lower boundary. The solution here is entirely analytical. Since the fields without random perturbation are conservative and exert no net torque about the sun, both energy and angular momentum are conserved which when combined with geometric properties of ellipses yield initial velocity as a function of semi-major axis and initial position.[[2]]

$$v = \sqrt{GM\left(\frac{2}{r} - \frac{1}{a}\right)} \qquad (2)$$

It is initially tempting to take an initial condition and rotate it by arbitrary angles to generate random orbits. However, since homogeneous densities are not homogeneous in r, it is

better to calculate a random point inside a cube until that point is also encompassed by the sphere, and then determine a random, orthogonal velocity. If initial conditions are determined in this fashion, the distribution of points inside the sphere displays banding corresponding to the differential of volume with respect to r, and banding caused by solid angle approximations.

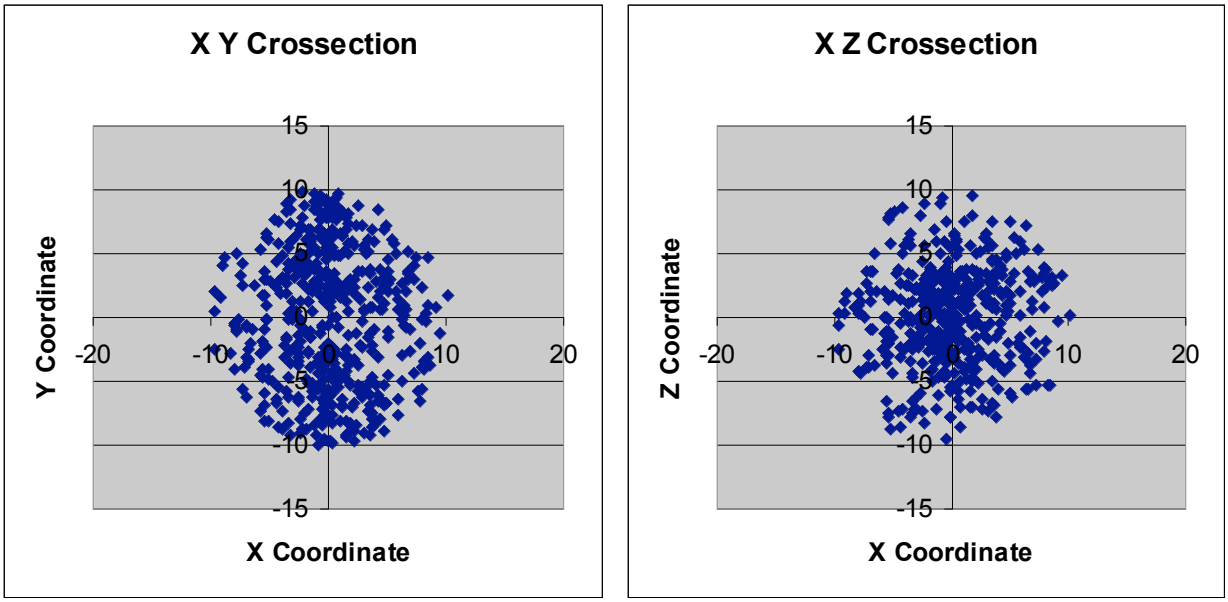

Figure 5: Non-Homogeneous Cross-Sections

Thus, to overcome this issue it is necessary to develop a technique to generate initial conditions which correspond to a homogeneous number distribution in the cloud. One solution is to find a random point in a .125 pc^3 region, and then determine a velocity magnitude corresponding to a random semi-major axis of a particle starting at this position. Then, a method is needed for determining a random unit vector orthogonal to the initial position. Scatter plots of these corrected initial positions are included in Appendix A

Determining a random unit vector orthogonal to the initial position can be done in the following manner. First, it is necessary to define an ortho-normal coordinate system with one coordinate axis pointing in the same direction as the initial position vector. Thus, we define a coordinate system:

$$x' = \frac{1}{|\hat{r} \times x|} \hat{r} \times x$$

$$y' = \frac{1}{|\hat{r} \times x|} \hat{r} \times \hat{r} \times x$$

$$z' = \hat{r}$$

Thus, if we define a vector combination of x' and y' with magnitude given by (2) we receive a set of random initial conditions which remain stably inside the region of interest if they are unaffected by external actors.

In terms of velocity distribution, the function is not flat. Given that the function is generated by two random variables (initial distance and semi-major axis) the surface distribution maximizes at a value of $4\times10^{-6}\,10kAU/yr$. A histogram of the initial conditions gives the distribution:

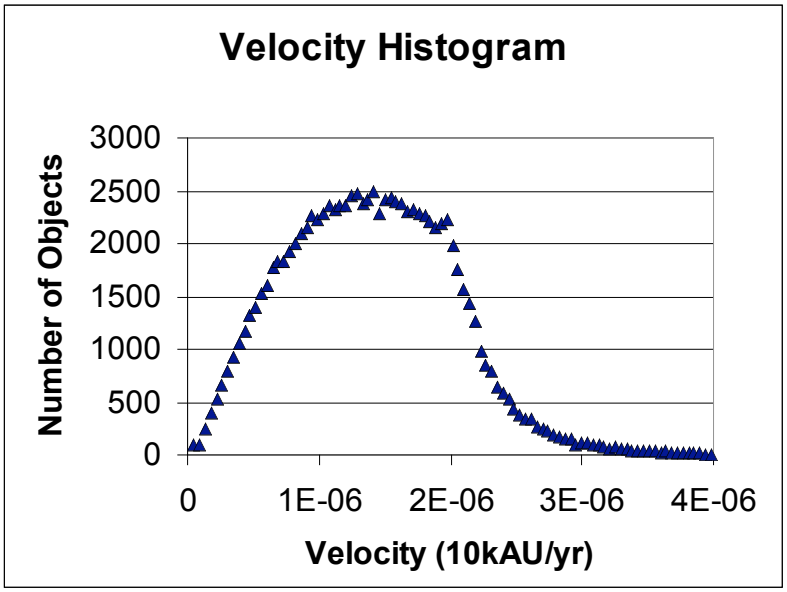

Figure 6: Velocity Histogram

The Acceleration Functions:

The Galactic Bulge:

Depending upon the particular model chosen there are many different options for the gravitational potential emitted by the galactic bulge. One popular model utilized by Masi gives a potential: $V(r) = -\frac{M_{BG}G}{\sqrt{r^2 + r_b^{\,2}}}$.[[3]]

Using the relation $a = -\nabla V$, the acceleration exerted by the bulge on an object is given by $a = -\frac{rM_{BG}G}{(r^2 + r_b^{\,2})^{1.5}}\hat{r}$. Where r is the position of the object and r_b is the radius of the galactic core.

The Galactic Disc:

The acceleration functions due to the disc are derived via Gauss' Law for gravitation. Since the desired geometry is that of a cylinder, and, as such, is proportional to displacement from z = 0. Given a homogenous mass distribution, this gives rise to the acceleration $a = -4\pi G\rho z$.[[2]] This effectively "squeezes" comets out of high z-coordinate ranges. Additionally, this force causes the sun itself to oscillate across the x-y galactic plane.

The MACHO sub-haloes:

MACHO sub-haloes interact as point masses to all comets outside the halo itself. The radius of a MACHO is determined by a critical density and its mass. Thus, by using the density function to determine a mass enclosed value, Gauss's method gives acceleration functions for passing haloes. $a = \frac{M_{enc} G}{(r_h - r_c)^{1.5}}$.

Thus, the total acceleration function for a comet given our simulation parameters is:

$$a = -\frac{M_* G}{r_c^3} r_c - \frac{(r_c - r_{BG}) M_{BG} G}{((r_c - r_{BG})^2 + r_b^2)^{1.5}} - 4\pi\rho(r_c + r_*)\hat{z} + \sum_{i=0}^{n} \frac{M_{enc_i} G}{(r_{h_i} - r_c)^{1.5}} (r_{h_i} - r_c)$$

Data:

The raw data from the simulation are output in the form of a text file of ordered triples representing the progressing position vectors over time. From these ordered triples it is possible to ascertain several useful physical quantities.

One useful analytical tool is the evolution of cloud population with time. This trend gives a good measure of the relative effectiveness of different effects. Additionally, these figures can be used to form a heuristic to test whether or not the simulation behaves similarly to expectations; by comparing similar order of magnitude effects and determining whether or not they have same order of magnitude effects on the cloud population.

However, in terms of checking the behavior of both the simulator and the simulated objects, the most useful intuitive tool is a three dimensional plot of the space curve traced out by the data points. Unfortunately, good plotting software for three dimensional data sets is somewhat lacking. To overcome this we wrote our own plotting software to show orbit time evolution and output this evolution as a set of bitmap files which could then be sequenced into an animation showing the motion of the simulated objects through time. Plots of unperturbed orbits display the usual Keplerian kinematics. These objects follow elliptical trajectories, and have a standard deviation from their expected semi-major axes of 0.0001 10kAU. A few of these trajectories degenerate or display periodic expansive behavior. This is caused by numerical error. Since, in our simulation, we opted to utilize a fixed time step, some orbits because of small initial position and high eccentricity, experience an accelerating deviation from the analytical solution, which in this case is known. This suggests proper function of the integration routines. Plots of the Bulge, Disc and their combination are useful in determining the manner in which tidal forces interact with Oort Cloud Objects. The Galactic Disc tends to have a more observable effect since it carries a larger range of force magnitudes and since this range can extend to much higher values than those of the Bulge objects with initial conditions in this range are more obviously perturbed.

The superposition of the two effects gives a slightly smaller number of escaping orbits than the simple addition of escaping orbit totals for the individual effects. This suggests an overlap in unstable initial conditions for both effects.

Both the plots and the population evolutions are useful in their own rite, but since the only observable quantity tying the simulation to the solar system is the number of orbits which

penetrate the planetary region of the solar system. Experimentally speaking, astronomers detect approximately one of these comets every day.[[6]] Thus, by attaining impact parameters for the destabilized orbits, it is possible to compare simulated flux with experimental. In practice, determining these values is best achieved by utilizing numerical interpolation between the raw data points, and then determining whether or not the interpolated points fall inside the observable region. Using this method, the three considered galactic interactions give a flux of observable objects over a period of 500 Myr in Table 1.

Interaction	Total Observed Events	Corrected Events	Yearly Rate
Sun Alone	0	0	0
Sun and Bulge	18	1800000000	36
Sun and Disc	11	1100000000	22
Sun Bulge and Disc	14	1400000000	28

Table 1: Observable Flux without Dark Matter

This figure seems low, but a correction needs to be made to reflect the fact that our simulations were of only 1000 objects, while astronomers estimate a population of a trillion objects. Using this correction ratio, the corrected simulated fluxes become: 0, 360, 220, and 280. It is difficult to ascribe error boundaries on these figures since the exact mechanics of comet injection in the particular system is not well-known.

Accuracy of the Simulation:

It is very difficult to ensure that a numerical simulation of a system with no analytical approach is behaving properly. Since the new paths cannot be compared to an expected function, deviation of the simulation from the actual simulation can at best be limited to a range of values dependent upon the chosen time step. Thus, a useful measure of error in a simulation of a conservative system is a time evolution of mechanical energy in the system. Thus, by determining percentage change in the energy from initial conditions to final ones gives a good measure of the accumulated numerical error over time. With a time step of 100 years and our implementation of Runge-Kutta we see energy evolutions of 0.00001% in solar simulations, 0.00002% in disc simulations, 0.00001% in bulge simulations, and 0.000025% in combined effect simulations. Thus, it is reasonable to expect the simulation yields physical results in the selected time frame.

In the Future:

While the work done here represents a significant step forward in the understanding of galactic structure and its observable effects on the solar system, more simulations are needed. It would be interesting to explore the effects of curved halo trajectories. Additionally, since the Oort Cloud Objects are posited to be so numerous, larger scale simulations of 10^5 or more objects may give a better idea of the continuous flux effects. Since our simulations were of a relatively small number of objects flux into the inner solar system was only meaningful as a measure of average flux over time, however, with a larger scale simulation it would be possible to determine the dynamic behavior of the perturbative forces and more specifically, their effects

on observable interaction rates. Additionally, implementation of an adaptive step-size method would enable exploration of comets' behavior within the inner solar system. However, to truly explore these effects, modeling of the gas giant planets would be necessary to observe the gravitational shielding effects they provide.

Further, it may be interesting to explore the manner in which initial distributions of both position and semi-major axis affect inner solar system comet injection rates as well as cloud population evolutions. Theoretical material on this subject is notably lacking, since the cloud has small mass and is very distant, external measurement of the distribution is difficult.

This weakness could be compensated for by doing a simulation of the early solar system to determine the distribution of the resulting cloud. Additionally, the resulting velocity distribution could be compared to that generated by the algorithm presented in this work to determine how similar the resultant cloud conditions are to the projected Keplerian solution. Furthermore, a simulation of the Oort Cloud formation and then its subsequent time evolution would allow correlation of simulation injection rates to experimental injection rates to possibly give a rough determination of the validity of the chosen galactic model. More critically, it is unclear whether or not these initial Keplerian conditions could ever arise out of solar system formation. Since it is unreasonable to assume only solar forces were important in the formation of the cloud, modeling of this process may yield a significantly different distribution of velocity magnitudes, semi-major axes, and initial positions.

References:

1. Oort, J. H., *The structure of the cloud of comets surrounding the Solar System and a hypothesis concerning its origin*, Bull. Astron. Inst. Neth., vol. 11, p. 91-110 (1950)
2. Fernandez, Juilo A. *Comets,: Nature, Dynamics, Origin, and Cosmological Relevance.* The Netherlands: Springer 2005.
3. Masi, M., *Dynamical effects of the radial galactic tide on an Oort cloud of comets for stars with different masses and varying distances from the galactic center,* eprint arXiv:astro-ph/0403599, March 2004.
4. Diemand, J et al, *Earth Mass Dark Matter Halos as the first structures in the Early Universe*, arXiv:astro-ph/0501589 v1 27, Jan 2005
5. Lewin, J.D., and Smith, P.F., *Review of Mathematics, Numerical Factors, and Corrections for Dark Matter Experiments Based on Elastic Nuclear Recoil*, *Astropart. Phys.*, **6**, 87-112, (1996).
6. Francis, P. J., *The Demographics of Long Period Comets*, Astrophys.J. 635 (2005) 1348-1361
7. Rubin, Vera C. & W. Kent Ford, Jr., *Rotation of the Andromeda Nebula from a Spectroscopic Survey of Emission Regions*, Ap.J. 159, 379-404 (1970).
8. Dehnen, W et al. *The velocity dispersion and mass profile of the Milky Way*. Mon. Not. R. Astronomical Society. April 2005.
9. Greist, K. "The Nature of Dark Matter." Dark Matter in the Universe. Ed. Bonometto et al. Enrico Fermi International School of Physics 1995. 343-347.
10. Alcock et al. 1996

Appendix A:

Generation functions for randomized trajectories between two concentric spherical shells. To generate random trajectories which remain between two concentric spheres it is necessary to accomplish three tasks, find a relation between velocity and elliptical constants, use some properties of ellipses to limit these constants to place the trajectory inside the desired region, and generalize these findings to the three dimensional case.

In two dimensions the equations of motion for a test particle in a bound can be shown to form an elliptical trajectory. If we set a coordinate system such that the semi major axis lies along the x-axis with the sun at the origin.

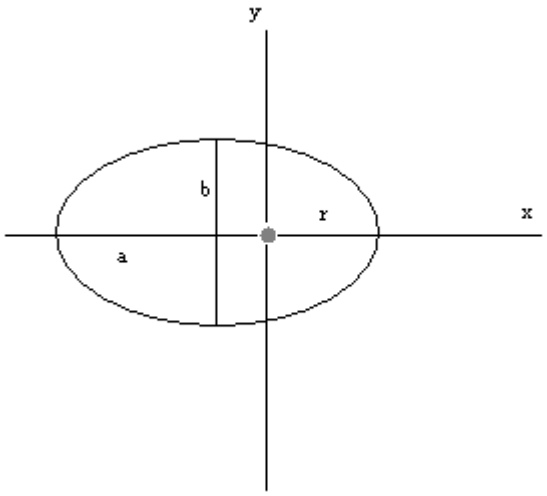

Figure 7: Elliptical Properties

Since the forces involved are conservative:

$$\frac{1}{2}mv_1^2 - \frac{GM}{x_{\min}} = \frac{1}{2}mv_2^2 - \frac{GM}{x_{\max}} \qquad \text{(A1)}$$

Additionally, no external torque is present in the system:

$$v_2 x_{\min} = v_1 x_{\max} \qquad \text{(A2)}$$

Using some knowledge about ellipses it is possible to refine the system further. Primarily, $x_{\min} = x_{\max} - 2a$. [[A2]] then reduces to give a substitution for v_2:

$$v_2 = \frac{v_1 x_{\max}}{(x_{\max} - 2a)} \qquad \text{(A3)}$$

Using [[A3]] in [[A1]] we get [[2]]:

$$v_1^2 - \left(\frac{v_1 x_{\max}}{(x_{\max} - 2a)}\right)^2 = 2GM\left(\frac{1}{x_{\max} - 2a} - \frac{1}{x_{\max}}\right)$$

$$v_1^2\left(\frac{(x_{\max}-2a)^2-x^2{}_{\max}}{(x_{\max}-2a)^2}\right)=2GM\left(\frac{2a}{x_{\max}(x_{\max}-2a)}\right)$$

$$v_1^2=2GM\left(\frac{2a(x_{\max}-2a)}{4ax_{\max}(-x_{\max}+a)}\right)$$

$$v_1^2=GM\left(\frac{1}{(a-x_{\max})}-\frac{-2a}{x_{\max}(a-x_{\max})}\right)=\sqrt{GM\left(\frac{2}{x_{\max}}-\frac{1}{a}\right)} \qquad \text{(A4)}$$

Given this relation it is important to restrict the values of a such that the initial velocity is real.

$$a_{\max}=2x_{\max} \qquad \text{(A5)}$$

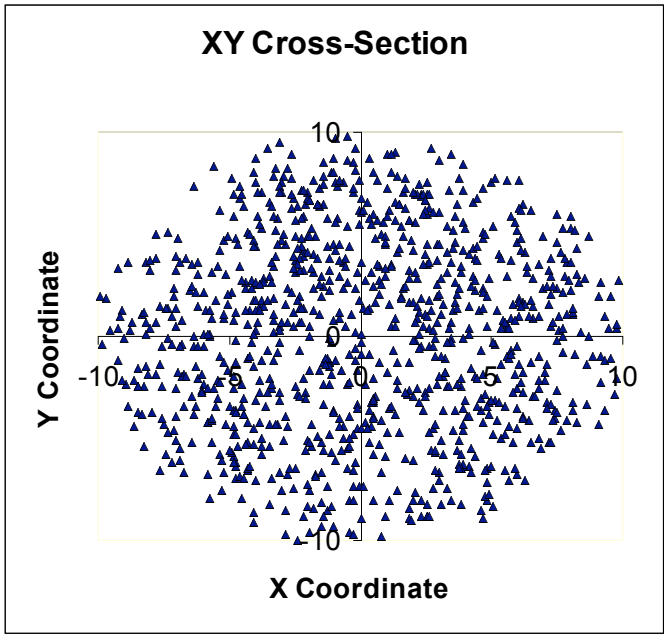

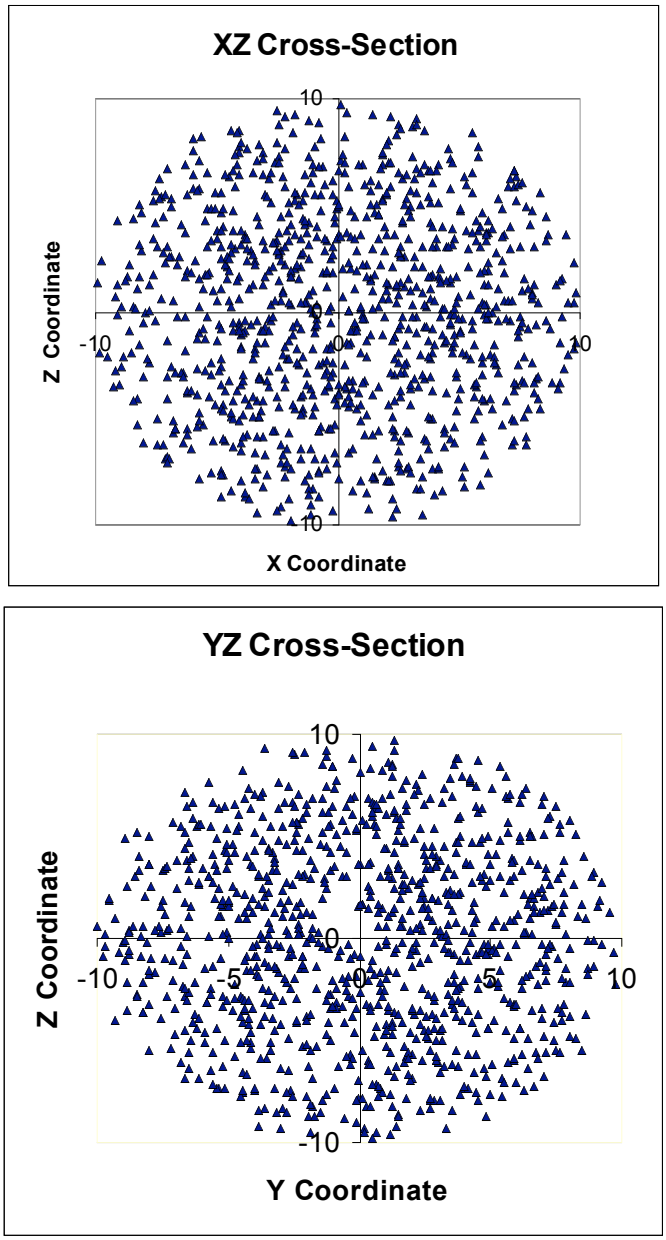

Figure 8: Homogeneous Cross Sections

Appendix B:

The distribution of mass in a MACHO is given by the distribution:

$$\rho(r) = \rho_0 r^{-\gamma} \tag{B1}$$

Where γ is a number between 1 and 2. Thus, the mass function of the MACHO is given by an integration of ρ.

$$M(r) = \frac{\rho_0}{3-\gamma} r^{3-\gamma} \tag{B2}$$

Thus the acceleration field exerted by a single MACHO is given by:

$$a(r) = \begin{cases} \dfrac{M_H G(r_h - r)}{(r_h - r)^{1.5}} & |r_h - r| > R_{\max} \\ \dfrac{\rho_0}{3-\gamma} G\,|r_h - r|^{1.5-\gamma}\,(r_h - r) & |r_h - r| \le R_{\max} \end{cases} \qquad \text{(B3)}$$

Appendix C:

Comet Generation Algorithm:

```
Comet::Comet()
{

	double rmax = 0.5f * 20.62;
	double rmin = 0.1f * 20.62;

	double v,r,a;

	while ( !InCloud(position*position,rmax,rmin))
	{

		position[0] = 2.0f*rmax*Rand() - rmax;
		position[1] = 2.0f*rmax*Rand() - rmax;
		position[2] = 2.0f*rmax*Rand() - rmax;

	}
	r = sqrt(position*position);


	a = r*Rand() + r;
	v = sqrt(G * (2.0f/a - 1.0f/r));


	Vector x_p,y_p;
	Vector x_h(1,0,0);

	x_p = Cross(position, x_h);
	y_p = Cross(position,x_p);
	x_p = (1.0f/sqrt(x_p*x_p))* x_p;
	y_p = (1.0f/sqrt(y_p*y_p)) * y_p;

	double thet = 2.0f* 3.14159 * Rand();

	velocity = v*sin(thet) * x_p + v*cos(thet) * y_p;



}
```

Runge-Kutta 4th order Vector Form:

```
Vector RungeKutta(Comet C, Bulge B, Disc D, Sun S, HaloList Hlist,double h,
int it)
{
      Vector k[4];
      double time = it * h;

      k[0] = h * S.Grav(C.position);
      if (b) k[0] = k[0] + h * B.Grav(C.position);
      if (d) k[0] = k[0] + h * D.Grav(C.position);
      if (ha) k[0] = k[0] + h * Hlist.a(time,C.position - S.position);


      k[1] = h * S.Grav(C.position + 0.5f * h *(C.velocity + (0.5f * k[0])));
      if (b) k[1] = k[1] + h * B.Grav(C.position + 0.5f*h*(C.velocity + 0.5f
*k[0]));
      if (d) k[1] = k[1] + h * D.Grav(C.position + 0.5f*h*(C.velocity + 0.5f
*k[0]));
      if (ha) k[1] = k[1] + h * Hlist.a(time + h/2.0f,C.position -
S.position+ 0.5f*h*(C.velocity + 0.5f * k[0]));


      k[2] = h * S.Grav(C.position + 0.5f*h*(C.velocity + (0.5f  * k[1])));
      if (b) k[2] = k[2] + h * B.Grav(C.position + 0.5f*h*(C.velocity + 0.5f
* k[1]));
      if (d) k[2] = k[2] + h * D.Grav(C.position + 0.5f*h*(C.velocity + 0.5f
* k[1]));
      if (ha) k[2] = k[2] + h * Hlist.a(time + h/2.0f,C.position - S.position
+ 0.5f * h * (C.velocity + 0.5 * k[1]));

      k[3] = h * S.Grav(C.position + h * (C.velocity  +  k[2]));
      if (b) k[3] = k[3] + h * B.Grav(C.position + h * (C.velocity + k[2]));
      if (d) k[3] = k[3] + h * D.Grav(C.position + h * (C.velocity + k[2]));
      if (ha) k[3] = k[3] + h * Hlist.a(time + h,C.position  - S.position + h
* (C.velocity + k[2]));

      return (1.0f/6.0f) * k[0] + (1.0f/3.0f)*k[1] + (1.0f/3.0f)*k[2] +
(1.0f/6.0f)*k[3];
}
```

Linear Algebra Package:

```
Vector::Vector()
{
      for (int i = 0; i < 3; i++)
      {
            data[i] = 0;
      }
}

Vector::Vector(double a, double b, double c)
{
      data[0] = a;
      data[1] = b;
      data[2] = c;
}
```

```
Vector Vector::operator +(Vector v2)
{
	Vector temp;
	temp[0] = data[0] + v2[0];
	temp[1] = data[1] + v2[1];
	temp[2] = data[2] + v2[2];

	return temp;
}

Vector Vector::operator -(Vector v2)
{
	return *this + (v2*(-1.0f));
}

Vector Vector::operator *(double c)
{
	Vector temp = *this;
	for (int i = 0; i < 3 ; i++)
	{
		temp.data[i] *= c;
	}
	return	temp;
}
double Vector::operator *(Vector v2)
{
	double sum = 0;
	for ( int i = 0; i < 3; i++)
	{
		sum += data[i] * v2[i];
	}
	return sum;
}
double & Vector::operator [](int i)
{
	return data[i];
}

Vector operator *(double c, Vector v)
{
	return v * c;
}

ostream & operator <<(ostream& out, Vector v)
{
	return out << v[0] << "\t" << v[1] << "\t"<< v[2] << endl;
}

istream& operator >>(istream& in, Vector& v)
{
	return in >> v[0] >> v[1] >> v[2];
}

Vector Cross(Vector v1, Vector v2)
{
```

```
	Vector temp(v1[1] * v2[2] - v1[2] * v2[1],-v1[0]*v2[2] +
v1[2]*v2[0],v1[0]*v2[1] - v1[1]*v2[0]);

	return temp;
}
ostream & operator <<(ostream& out, Matrix M)
{
	out<<M[0]<<M[1]<<M[2];
	return out;
}
Matrix::Matrix()
{
	Vector temp;
	for ( int i = 0; i < 3; i++)
	{
		data[i] = temp;
		data[i][i] = 1;
	}

}

Matrix Matrix::operator *(double c)
{
	Matrix M = *this;
	for ( int i = 0; i < 3; i++)
	{
		for ( int j = 0; j < 3; j++)
		{
			M[i][j] *= c;
		}
	}
	return M;
}

Matrix Matrix::operator *(Matrix M)
{
	Matrix M_t;
	for ( int i = 0; i < 3; i++)
	{
		for ( int j = 0; j < 3; j++)
		{
			M_t[i][j] = 0;
			for ( int k = 0; k < 3;k++)
			{
				M_t[i][j] += data[i][k] * M[k][j];
			}
		}
	}
	return M_t;
}

Vector Matrix::operator *(Vector v)
{
	Vector ret;
	ret[0] = data[0] * v;
	ret[1] = data[1] * v;
	ret[2] = data[2] * v;
```

```
	return ret;
}

Matrix Matrix::operator +(Matrix M)
{
	Matrix ret;
	for ( int i = 0; i < 3; i++)
	{
		for ( int j = 0; j < 3; j++)
		{
			ret[i][j] = data[i][j] + M[i][j];
		}
	}
	return ret;
}

Matrix Matrix::operator -(Matrix M)
{
	return *this + (M* (-1.0f));
}

Vector & Matrix::operator [](int i)
{
	return data[i];
}

Matrix operator *(double c, Matrix M)
{
	Matrix M1 = M;
	for ( int i = 0; i < 3; i++)
	{
		M1[i] = c* M[i];
	}
	return M1;
}

Matrix Matrix::operator *=(Matrix M)
{
	return *this * M;
}


Matrix rot_x(double theta)
{
	Matrix rot;

	double c = cos(theta);
	double s = sin(theta);


		Vector temp(0,c,s);
		Vector temp2(0,-s,c);
		Vector temp3(1,0,0);
		rot[1] = temp;
		rot[2] = temp2;
```

```
            rot[0] = temp3;

      return rot;

}
Matrix rot_y(double theta)
{
      Matrix rot;

      double c = cos(theta);
      double s = sin(theta);



            Vector temp(c,0,-s);
            Vector temp2(s,0,c);
            Vector temp3(0,1,0);
            rot[0] = temp;
            rot[2] = temp2;
            rot[1] = temp3;

      return rot;

}
Matrix rot_z(double theta)
{
      Matrix rot;

      double c = cos(theta);
      double s = sin(theta);



            Vector temp(c,s,0);
            Vector temp2(-s,c,0);
            Vector temp3(0,0,1);
            rot[0] = temp;
            rot[1] = temp2;
            rot[2] = temp3;

      return rot;

}
Matrix rot_allaxes(Vector v)
{

      return rot_y(v[1]) * rot_z(v[2])* rot_x(v[0]);
}
```